Atmos. Chem. Phys. Discuss., https://doi.org/10.5194/acp-2018-159
Manuscript under review for journal Atmos. Chem. Phys.
Discussion started: 13 April 2018

Atmospheric Chemistry and Physics Discussions

Production of particulate brown carbon during atmospheric aging of wood-burning emissions

Nivedita K. Kumar[1], Joel C. Corbin[1*], Emily A. Bruns[1], Dario Massabó[2], Jay G. Slowik[1], Luka Drinovec[3,4], Griša Močnik[3,4], Paolo Prati[2], Athanasia Vlachou[1], Urs Baltensperger[1], Martin Gysel[1], Imad El-Haddad[1] and André S. H. Prévôt[1]

[1]Laboratory of Atmospheric Chemistry, Paul Scherrer Institute, 5232 Villigen, Switzerland
[2]Department of Physics & INFN, University of Genoa, via Dodecaneso 33, 16146, Genova, Italy
[3]Aerosol d.o.o, Kamniška 41, 1000 Ljubljana, Slovenia
[4]Condensed Matter Physics, Jožef Stefan Institute, 1000 Ljubljana, Slovenia
*Now at National Research Council Canada, Ottawa, Canada

Correspondence to: I. El-Haddad (imad.el-haddad@psi.ch), A. S. H. Prévôt (andre.prevot@psi.ch)

ABSTRACT

We investigate the optical properties of light-absorbing organic carbon (brown carbon) from domestic wood combustion as a function of simulated atmospheric aging. At shorter wavelengths, light absorption by brown carbon from primary organic aerosol (POA) and secondary organic aerosol (SOA) formed during aging was around 10 % and 20 %, respectively, of the total aerosol absorption (brown carbon plus black carbon). The mass absorption cross-section (MAC) determined for black carbon (BC, 13.7 $m^2 g^{-1}$ (geometric standard deviation GSD = 1.1) at 370 nm) was consistent with that recommended by Bond et al. (2006). The corresponding MAC of POA (5.5 $m^2 g^{-1}$ (GSD =1.2)) was higher than that of SOA (2.4 $m^2 g^{-1}$ (GSD = 1.3)) at 370 nm. However, SOA presents a substantial mass fraction, with a measured average SOA/POA mass ratio after aging of ~5 and therefore contributes significantly to the overall light absorption, highlighting the importance of wood-combustion SOA as a source of atmospheric

Atmos. Chem. Phys. Discuss., https://doi.org/10.5194/acp-2018-159
Manuscript under review for journal Atmos. Chem. Phys.
Discussion started: 13 April 2018

Atmospheric Chemistry and Physics Discussions

brown carbon. The wavelength dependence of POA and SOA light absorption between 370 nm and 660 nm is well described with absorption Ångström exponents of 4.6 and 5.6, respectively. UV-visible absorbance measurements of water and methanol-extracted OA were also performed showing that the majority of the light-absorbing OA is water insoluble even after aging.

1. INTRODUCTION

Atmospheric aerosols contribute to radiative forcing either directly by absorbing and scattering light or indirectly by acting as cloud-condensation and ice nuclei. While black carbon (BC) from combustion processes is the most efficient light-absorbing aerosol component, organic aerosols (OA) may also absorb solar radiation (Alexander et al., 2008; Chen and Bond, 2009; Kirchstetter et al., 2004). This light-absorbing OA, denoted as brown carbon (BrC), absorbs most strongly at shorter UV-visible wavelengths (Andreae and Gelencsér, 2006; Hoffer et al., 2005). Global chemical-transport model estimates indicate that the BrC contribution to the positive radiative forcing of climate by anthropogenic aerosols may not be negligible (Feng et al., 2013; Jo et al., 2016; Lin et al., 2014; Wang et al., 2014).

Unlike BC, whose light absorption properties are relatively constant across sources (Bond et al., 2013), BrC is composed of a wide range of largely unknown compounds, which exhibit highly variable spectral dependence and absorption efficiencies. For example, reported imaginary indices of refraction for different organic species, which describe the absorption of these compounds, span two orders of magnitude (Lu et al., 2015). Because it is impractical to experimentally separate BrC from non-absorbing OA, optical properties are typically determined for the bulk OA of a given source. The large variability of BrC fraction in combustion aerosol may contribute to the wide variation in reported properties of BrC containing OA.

Biomass burning OA, which contributes two-thirds of the global budget of directly-emitted primary OA (POA), is expected to be a considerable source of BrC (Chakrabarty et al., 2010; Hecobian et al., 2010; Lack and Langridge, 2013; Liu et al., 2014). The variability in reported light absorption properties of biomass burning OA with fuel type and burn conditions remains a major obstacle complicating its treatment in climate models (Lu et al., 2015; Saleh et

al., 2013). Residential biomass burning is typically characterized by a more efficient combustion, than open burning. Residential wood burning represents a substantial contribution to anthropogenic combustion emissions (Bond et al., 2013), especially in urban atmospheres, and is considered the largest source of OA in Europe during winter (Denier Van Der Gon et al., 2015).

Upon photo-oxidation, biomass-burning emissions produce secondary organic aerosol (SOA) at concentrations similar to or exceeding the primary organic aerosol (POA) (Bertrand et al., 2017; Bruns et al., 2015, 2016; Corbin et al., 2015a; Grieshop et al., 2009). There is a growing body of evidence that light absorption by OA change with OH exposure (aging) owing to the production of secondary BrC or to the transformation of primary BrC (Heringa et al., 2011; Lee et al., 2014; Zhao et al., 2015). However, these effects have not yet been systematically investigated and must be quantified to assess the climate effects of primary and aged biomass burning OA.

Here, we show that both POA and SOA from residential biomass burning emissions aged in controlled smog chamber experiments contain BrC. Wavelength dependent, mass-normalized absorption cross-sections (MACs) of POA and SOA are presented from online aerosol measurements as a function of aging for the first time. Complementary measurements of filter-extract absorbance (conducted in different solvents) are used to obtain the imaginary refractive index and to investigate the solubility of BrC in fresh and aged OA. While results presented here are related to flaming residential wood combustion emissions and cannot therefore be generalized, the approach used can be extrapolated for the characterization and quantification of the contribution of BrC in other primary and aged emissions.

2. METHODS

2.1 Smog chamber experiments

Laboratory measurements were conducted in an 8 m^3 Teflon smog chamber (Bruns et al., 2015; Platt et al., 2013) installed within a temperature-controlled housing. Conditions in the chamber were maintained to represent winter time in Europe, i.e. relative humidity ranging between 50 – 90%, at 263 K (Bruns et al., 2015, 2016). Beech wood was combusted in a residential wood stove. Primary emissions were sampled through heated lines at 413 K, diluted by a factor of ~14 using an ejector diluter (DI-1000, Dekati Ltd.), then sampled into the chamber, which provided an

additional ten-fold dilution. The overall dilution was a factor of 100 to 200. As we aimed to sample only flaming-phase emissions into the chamber, samples were taken when the modified combustion efficiency (ratio of CO_2 to the sum of CO and CO_2) was > 0.90. Despite maintaining the same combustion conditions, the resulting organic fraction in the different samples was highly variable, indicating that these samples are representative of a mixture of pre-ignition and flaming emissions (with varying contributions of each combustion stage).

After injection of the primary emissions and stabilization of the concentrations, nitrous acid (HONO) was continuously added, which dissociates upon irradiation (λ<400 nm) and forms the hydroxyl radical (OH). Then, 9-times deuterated butanol sample (butanol- D9, 98%, Cambridge Isotope Laboratories) was subsequently injected into the chamber. The decay of butanol-D9 was used to infer the time-resolved OH exposure of the sampled aerosol (Barmet et al., 2012). The chamber was exposed to UV lights for ~3.5 hours.

Particles were collected onto filters (47 mm Tissue-quartz, Pall Corporation, 26 L min^{-1} for 30-32 min) for offline optical measurements and the determination of elemental carbon (EC) mass. Three filters were collected during each experiment, namely i) a primary aerosol filter sample ("primary"), ii) a slightly aged aerosol ("Aged1", OH exposure ~ $1x10^7$ molecules cm^{-3} h), collected 30 minutes after the UV lights were switched on, and iii) an aged aerosol ("Aged2", OH exposure ~ $4x10^7$ molecules cm^{-3} h), collected at the end of the experiment (see Figure S1 for the sampling periods). A charcoal denuder was installed upstream of the filter sampler to remove organic gases. Filters were stored at 253K until analysis.

In addition to the characterization of the particle optical properties detailed in the next section, a set of online and offline techniques were used for the characterization of the gaseous and particulate emissions before and after aging. The non-refractory particle size-segregated chemical composition was measured with a high resolution (HR) time-of-flight aerosol mass spectrometer (AMS) (DeCarlo et al., 2006). Details related to the AMS data analysis and calibration can be found elsewhere (Bruns et al., 2015, 2016). A scanning mobility particle sizer was used to measure the size distribution of the evolving aerosol. Organic gases were monitored by a proton transfer reaction time-of-flight mass spectrometer (PTR-MS, [H_3O^+] reagent ion, Ionicon Analytik GmbH) (Bruns et al., 2017), following the same procedure as in Klein et al. (2016). Additionally, elemental carbon (EC) mass concentration was measured offline using a sunset thermo-optical analyzer, following the EUSAAR2 protocol (Cavalli et al., 2010).

Atmos. Chem. Phys. Discuss., https://doi.org/10.5194/acp-2018-159
Manuscript under review for journal Atmos. Chem. Phys.
Discussion started: 13 April 2018

Atmospheric Chemistry and Physics Discussions

2.2 Optical measurements

Aethalometer. A dual-spot aethalometer (Magee Scientific aethalometer AE33, Aerosol d.o.o.) was used for real-time aerosol light attenuation measurements at seven wavelengths (λ = 370, 470, 520, 590, 660, 880 and 950 nm) (Drinovec et al., 2015). The instrument measures the attenuation coefficient (b_{ATN}) of a light beam transmitted through a filter tape loaded with aerosol samples. The use of the sampling flow (here, 2 L min^{-1}), integration time for the measurement (here, 1 minute), and automated dual-spot loading compensation to obtain b_{ATN} has been described by Drinovec et al. (2015).

The loading compensated b_{ATN} was used to infer the aerosol absorption coefficient, b_{abs}, using a constant wavelength independent correction factor C, which accounts for multiple scattering within the filter matrix (Weingartner et al., 2003):

$$b_{abs}(\lambda) = b_{ATN}(\lambda)/C \quad (1)$$

The loading compensated b_{ATN} at 880 nm from the AE33 is further used to infer the equivalent-BC mass concentration, M_{eBC}:

$$M_{eBC} = \frac{b_{ATN}(880\ nm)}{\sigma_{ATN}(880\ nm)} \quad (2)$$

where σ_{ATN} is the mass attenuation cross-section of BC deposited on the filter of the AE33. M_{eBC} inferred from Equation 2 only equals the true BC mass concentration, M_{BC}, if the applied σ_{ATN} is identical to the true attenuation cross-section of BC, $\sigma_{ATN,BC}$, and if light attenuation at 880 nm is exclusively due to BC. $\sigma_{ATN,BC}(880\ nm)$ can be inferred from the true MAC of BC, MAC_{BC}, and the true C value:

$$\sigma_{ATN,BC}(880\ nm) = MAC_{BC}(880\ nm) * C \quad (3)$$

with MAC_{BC} being defined as:

$$MAC_{BC}(\lambda) = \frac{b_{abs,BC}(\lambda)}{M_{BC}} \quad (4)$$

where $b_{abs,BC}$ is the absorption coefficient due to BC.

122 The manufacturer default values are 1.57 for C and 12.2 $m^2 g^{-1}$ for σ_{ATN} at 880 nm, which corresponds to a
123 MAC_{BC}(880 nm) of 7.77 $m^2 g^{-1}$ at (Gundel et al., 1984 , Drinovec et al., 2015). However, these three parameters
124 depend on aerosol properties. Here, we have determined the C value by applying Equation 1 to b_{ATN} measured by the
125 aethalometer and the absorption coefficient, $b_{abs_{MWAA}}$, measured by a multi-wavelength absorbance analyser,
126 MWAA (Massabò et al., 2015; Massabò et al., 2013). The MAC_{BC}(880 nm) was determined using Equation 4 to
127 compare $b_{abs_{MWAA}}$ from the MWAA measurements with EC mass from the Sunset thermo-optical analyzer (see
128 Figure 1A&B and Section 4.1 for detailed discussion). Following this procedure, the MWAA and Sunset analyser
129 will be defined as reference methods for absorption coefficient and EC mass concentration, respectively. Note that
130 data from these reference methods were only available with low time resolution and for a subset of all samples.
131 Thus, the aethalometer anchored against these reference methods, was used to obtain the wavelength dependent
132 absorption coefficients and the eBC mass concentrations with high time resolution using Equations 1 and 2,
133 respectively. Processing the loading compensated AE33 attenuation coefficients with C value and MAC_{BC},
134 determined with independent MWAA and Sunset analyser measurements, ensures that the inferred $b_{abs}(\lambda)$
135 (Equation 1) and M_{eBC} (Equation 2) have minimal bias compared to respective true values.

136 **MWAA measurements.** The MWAA (Massabò et al., 2015; Massabò et al., 2013) was used as reference method
137 for the aerosol absorption coefficient. It measures the absorption coefficient $b_{abs_{MWAA}}(\lambda)$ of particles deposited on
138 on standard filter samples. It is composed of five laser diodes, with λ = 375, 407, 532, 635 and 850 nm, acting as
139 light sources and placed above the filter, an automated sample-changer, and three low-noise UV-enhanced
140 photodiodes. The first photodiode is placed behind the filter for the analysis of transmittance measurements, while
141 the other two photodiodes are positioned at specific angles between the sources and the loaded filter to perform
142 reflectance measurements. These transmittance and reflectance measurements are used together with a radiative
143 transfer model (Hänel et al., 1987) , which takes into account multiple scattering within the particle/filter layer, to
144 retrieve both the total optical thickness and the particle-filter-layer single scattering albedo, providing the absorption
145 coefficient $b_{abs_{MWAA}}(\lambda)$ values. These calculations largely follow the approach implemented in the multi-angle
146 absorption photometer (Petzold and Schönlinner, 2004).

147 **UV-visible absorbance measurements of extracted aerosols.** Filter samples were extracted for UV-visible
148 absorbance measurements in 10 mL ultrapure water or methanol in an ultrasonic bath for 20 min at 30 °C. Samples

Atmos. Chem. Phys. Discuss., https://doi.org/10.5194/acp-2018-159
Manuscript under review for journal Atmos. Chem. Phys.
Discussion started: 13 April 2018

Atmospheric Chemistry and Physics Discussions

were subsequently briefly vortexed (1 min) and filtered with 0.45 µm nylon membrane syringe filters following the procedure described in Daellenbach et al. (2016). Absorption spectra were measured from 280 to 500 nm using a UV-visible spectrophotometer (Ocean Optics) coupled to a 50-cm long-path detection cell (Krapf et al., 2016). Light attenuation by the OA in solution, $ATN_{\text{OA-sol}}$, at a given wavelength was recorded as the logarithm of the ratio of signal intensities of the reference (solvent) (I_0) and the sample (I), both corrected for background signals with the light source off. From $ATN_{\text{OA-sol}}$, the absorption coefficient of OA in solution, $b_{\text{abs,OA-sol}}(\lambda)$, can be quantified as:

$$b_{\text{abs,OA-sol}}(\lambda) = \frac{ATN_{\text{OA-sol}}(\lambda)}{l} \quad (5)$$

where l is the optical path length.

The absorbance measurements are aimed at inferring the imaginary part of the refractive index. For this, $b_{\text{abs,OA-sol}}(\lambda)$ is transformed to the absorption coefficient of the bulk OA in the pure form, $b_{\text{abs,OA-bulk}}$ (Sun et al., 2007):

$$b_{\text{abs,OA-bulk}}(\lambda) = b_{\text{abs,OA-sol}}(\lambda) \rho_{\text{OA}} \Big/ \frac{m_{\text{OA}}}{V_{\text{solvent}}} \quad (6)$$

where ρ_{OA} is the bulk density of OA (assumed to be 1.5 g cm^{-3}, typical of wood-burning OA; (Corbin et al., 2015a; Moosmüller et al., 2009; Sun et al., 2007)), m_{OA} is the extracted OA mass, and V_{solvent} is the solvent volume. The bulk absorption coefficient directly leads to the imaginary part of the OA refractive index, k_{OA}, in pure form (Moosmüller et al., 2009):

$$k_{\text{OA}}(\lambda) = b_{\text{abs,OA-bulk}}(\lambda) \frac{\lambda}{4\pi} \quad (7)$$

Inserting Equation 6 into Equation 7 eventually provides (Liu et al., 2015a):

$$k_{\text{OA}}(\lambda) = \frac{\lambda \rho_{\text{OA}} V_{\text{solvent}}}{4\pi m_{\text{OA}}} b_{\text{abs,OA-sol}}(\lambda) \quad (8)$$

The mass of organics dissolved in the solution could not be quantified. Therefore, we use an upper limit value for m_{OA}, approximated as the integral of AMS-measured OA mass concentration times sample flow rate over the filter-sampling period. Accordingly, the resulting k_{OA} values represent lower limits for the true values, as the OA extraction efficiency was not accounted for. Higher k_{OA} values based on online absorption coefficient measurements

compared to those calculated based on Equation 8 may be related to low OA extraction efficiency or to non-extractable highly absorbing material and results shall be discussed accordingly.

3. OPTICAL PROPERTIES ANALYSIS

3.1 Determination of absorption Ångström exponents and mass absorption cross-sections

In this section we describe the methodology adapted for the determination of the mass absorption cross-sections (MACs) for the different aerosol material from the Sunset, MWAA and aethalometer measurements. The assumptions and limitations underlying these calculations are clearly stated. We also explain the relationship between the MACs and the wavelength dependence of the overall absorption.

Definition of the absorption Ångström exponent . The wavelength dependence of the overall absorption due to both BC and BrC has often been described assuming a power law:

$$b_{abs}(\lambda) \propto \lambda^{-\alpha} \quad (9)$$

where α is the Ångström absorption exponent, often determined by fitting the absorption coefficient measurements across the entire wavelength range. Equation 9 is an empirical simplification, which breaks down when different components having different spectral dependence contribute to the absorption, e.g. a mix of BrC and black carbon (e.g., Moosmüller et al., 2011). In practice, different values of α would be obtained for different choices of λ ranges, and therefore we alternatively calculated two-wavelength absorption exponents according to

$$\alpha(\lambda, \lambda_{ref}) = -\frac{\ln\left(\frac{b_{abs}(\lambda)}{b_{abs}(\lambda_{ref})}\right)}{\ln\left(\frac{\lambda}{\lambda_{ref}}\right)} \quad (10)$$

where λ is a wavelength of interest (in nm) and λ_{ref} is the reference wavelength, here 880 nm. This reference wavelength was chosen, because BC is expected to fully dominate light absorption in this range (Laskin et al., 2015).

Atmos. Chem. Phys. Discuss., https://doi.org/10.5194/acp-2018-159
Manuscript under review for journal Atmos. Chem. Phys.
Discussion started: 13 April 2018

193 Black carbon is known to have an α between 0.9 and 1.1 (Bond et al., 2013; Kirchstetter et al., 2004; Liu et al.,
194 2015b), whereas BrC, which preferentially absorbs at shorter wavelength, has a higher α (Laskin et al., 2015; Saleh
195 et al., 2013). Thus, we interpret an increase of $\alpha(\lambda, \lambda_{ref})$ of the total aerosol as due to an increased contribution of
196 BrC to the total absorption. $\alpha(\lambda, \lambda_{ref})$ can potentially change due to other effects such as a wavelength dependent
197 lensing effect on absorption by BC (e.g., Lack and Langridge, 2013) or the restructuring of BC aggregates during
198 aging. The former effect was negligible under our conditions, as elaborated on below. The latter, if it occurs during
199 aging, would be attributed to SOA absorption in our approach. However, this is not an issue if our values are
200 accordingly applied in e.g. model simulations, following the same assumption as in our approach. This means that
201 the potential restructuring effects must implicitly be considered within the MAC(λ) of SOA, while the MAC(λ) of
202 BC must be kept fixed.

203 **3.2 Determination of MAC_{BC} and MAC_{POA} using the absorption Ångström exponent**

204 In a mixture of *n* absorbing species, the total absorption at any wavelength may be written as the sum of the
205 absorbance of each of the species. Accordingly, Equation 10 can be expressed for a multi-component system

206 $$\alpha(\lambda, \lambda_{\mathrm{ref}}) = \frac{1}{\ln(\lambda_{ref}/\lambda)} \ln\left(\frac{\sum_{i=1}^{n} b_{\mathrm{abs,i}}(\lambda)}{\sum_{i=1}^{n} b_{\mathrm{abs,i}}(\lambda_{ref})}\right) = \frac{1}{\ln(\lambda_{\mathrm{ref}}/\lambda)} \ln\left(\frac{\sum_{i=1}^{n} M_i MAC_{\mathrm{i}}(\lambda)}{\sum_{i=1}^{n} M_i MAC_{\mathrm{i}}(\lambda_{ref})}\right) \quad (11)$$

207 where the right hand side follows the general definition of MAC along the lines of Equation 4. M_i and MAC_i are the
208 mass concentration and MAC, respectively, of the i^{th} species, with *n* absorbing species in total. By considering that
209 the light absorption at λ_{ref} = 880 nm is exclusively due to BC, and by defining BC to be the n^{th} species, Equation
210 11 can be written as

211 $$\alpha(\lambda, 880nm) = \frac{1}{ln(880nm/\lambda)} ln\left(\frac{\mathrm{MAC_{BC}}(\lambda)}{\mathrm{MAC_{BC}}(880nm)} + \sum_{i=1}^{n-1} \frac{M_i \mathrm{MAC}_i(\lambda)}{b_{\mathrm{abs}}(880nm)}\right) \quad (12)$$

212 In equation 12, the summation now only goes over the n-1 organic species, which contribute to light absorption.
213 The fresh combustion aerosol exclusively contains BC and POA as absorbing species. For the data at time t_0 before
214 the start of photo-oxidative aging, Equation 12 simplifies to:

215 $$\alpha(t_0, \lambda, 880nm) = \alpha_{\mathrm{BC+POA}}(t_0, \lambda, 880nm)$$

$$= \frac{1}{\ln(880\text{nm}/\lambda)} \ln\left(\frac{\text{MAC}_{\text{BC}}(t_0,\lambda)}{\text{MAC}_{\text{BC}}(t_0,880nm)} + \frac{M_{\text{OA}}(t_0)\text{MAC}_{\text{POA}}(t_0,\lambda)}{b_{\text{abs}}(t_0,880nm)}\right) \quad (13)$$

In Equation 13, $M_{\text{OA}}(t_0)$ is the mass concentration of primary organic aerosol measured by the AMS at t_0. $\text{MAC}_{\text{BC}}(t_0,880\text{nm})$ was inferred from the MWAA and Sunset thermo-optical analysis and shown to be independent of the experimental conditions (Section 4.1; Figure 1A). Absorption coefficients $b_{\text{abs}}(t_0,\lambda)$ are obtained from the high time resolution attenuation measurements by the aethalometer referenced to the MWAA absorption measurements as described above. $\alpha(t_0,\lambda,880\text{ nm})$ is derived from $b_{\text{abs}}(t_0,\lambda)$ and $b_{\text{abs}}(t_0,880\text{ nm})$ using Equation 10.This leaves only 2 free parameters in Equation 13, $\text{MAC}_{\text{BC}}(t_0,\lambda)$ and $\text{MAC}_{\text{POA}}(t_0,\lambda)$. These were determined by fitting Equation 13 to $\alpha(t_0,\lambda,880\text{ nm})$, $M_{\text{OA}}(t_0)$, $\text{MAC}_{\text{BC}}(t_0,880\text{nm})$ and $b_{\text{abs}}(t_0,880nm)$ data measured in all experiments for fresh emissions at t_0. This approach contains the implicit assumption that the two MAC values are also independent of experimental conditions, and therefore these MACs should be considered as average values. The accuracy of these MAC values obviously depends on the accuracy of the absorption and mass measurements. First, a systematic bias in the C value potentially caused by a systematic bias in the MWAA measurements propagates to an identical bias in both $\text{MAC}_{\text{BC}}(t_0,\lambda)$ and $\text{MAC}_{\text{POA}}(t_0,\lambda)$. Second, a systematic bias in the Sunset EC mass measurements yields a corresponding inverse bias in $\text{MAC}_{\text{BC}}(t_0,\lambda)$, while $\text{MAC}_{\text{POA}}(t_0,\lambda)$ remains unaffected. Third, a systematic bias in the AMS POA mass yields a corresponding inverse bias in $\text{MAC}_{\text{POA}}(t_0,\lambda)$, while $\text{MAC}_{\text{BC}}(t_0,\lambda)$ remains unaffected. Equation 13 shows that α of the primary aerosol at a certain wavelength is largely driven by $\text{MAC}_{\text{POA}}(t_0,\lambda)$, i.e. the optical properties of POA, and by the ratio $\frac{M_{\text{OA}}(t_0)}{b_{\text{abs}}(t_0,880nm)}$, which reflects the relative contributions of POA and BC to total primary aerosol mass.

3.3 Determination of MAC_{SOA}

The MAC of SOA, MAC_{SOA}, can be generally defined as:

$$\text{MAC}_{\text{SOA}} = \frac{b_{\text{abs,SOA}}}{M_{\text{SOA}}} \quad (14)$$

where $b_{\text{abs,SOA}}$ and M_{SOA} are the absorption coefficient and mass concentration of SOA, respectively. In the aged aerosol, which contains the absorbing species BC, POA and SOA, $b_{\text{abs,SOA}}$ is the difference of the total absorption minus the absorption by POA and BC:

$$b_{\text{abs,SOA}}(t,\lambda) = b_{\text{abs}}(t,\lambda) - b_{\text{abs,POA+BC}}(t,\lambda) \quad (15)$$

Atmos. Chem. Phys. Discuss., https://doi.org/10.5194/acp-2018-159
Manuscript under review for journal Atmos. Chem. Phys.
Discussion started: 13 April 2018

241 The absorption by POA and BC in the aged aerosol is a priori unknown, but can be calculated under certain
242 assumptions. The first assumption is that SOA does not contribute to absorption at 880 nm:
243 $b_{\mathrm{abs,POA+BC}}(t, 880\ nm) \equiv b_{\mathrm{abs}}(t, 880\ nm)$. The second assumption is that the two-λ α values of primary emissions
244 do not change during aging $\alpha_{\mathrm{POA+BC}}(t, \lambda, 880\ nm) \equiv \alpha_{\mathrm{POA+BC}}(t_0, \lambda, 880\ nm)$. The latter approximation is based on
245 the underlying assumptions that the MAC of POA is not altered by aging and that the proportions of POA and BC
246 mass lost to the wall are identical. Under these assumptions $b_{\mathrm{abs,POA+BC}}$ becomes:

247 $$b_{\mathrm{abs,POA+BC}}(t, \lambda) = b_{\mathrm{abs}}(t, 880\ nm)\left(\frac{880\ nm}{\lambda}\right)^{\alpha_{\mathrm{POA+BC}}(t_0, \lambda, 880\ nm)} \quad (16)$$

248 Note that inferring $b_{\mathrm{abs,POA+BC}}(t, \lambda)$ from $b_{\mathrm{abs}}(t, 880\ nm)$ implicitly accounts for the decrease in the BC and POA
249 absorption due to wall losses.

250 M_{SOA} was obtained as total organic minus POA mass concentration:

251 $$M_{\mathrm{SOA}}(t) = M_{\mathrm{OA}}(t) - M_{\mathrm{POA}}(t) \quad (17)$$

252 The POA mass concentration in the aged aerosol can be inferred from the initial OA mass concentration in the fresh
253 emissions by accounting for the wall losses using Equation S1 and the wall loss time constant τ (see Section Wall
254 loss corrections in the SI):

255 $$M_{\mathrm{POA}}(t) = M_{\mathrm{OA}}(t_0)\exp(\tau^{-1}t) \quad (18)$$

256 Inserting Equations 15-18 into Equation 14 provides the final equation for inferring $\mathrm{MAC_{SOA}}$.

257 $$\mathrm{MAC_{SOA}}(t, \lambda) = \frac{b_{\mathrm{abs}}(t,\lambda) - b_{\mathrm{abs}}(t, 880\ nm)\left(\frac{880\ nm}{\lambda}\right)^{\alpha_{\mathrm{POA+BC}}(t_0, \lambda, 880\ nm)}}{M_{\mathrm{OA}}(t) - M_{\mathrm{OA}}(t_0)\exp(\tau^{-1}t)} \quad (19)$$

258

259 $\mathrm{MAC_{SOA}}$ can be calculated for every data point in time and for all aethalometer wavelengths from 370 to 660 nm
260 ($\mathrm{MAC_{SOA}}$ defined to be zero at λ ≥ 880 nm), as all quantities on the right hand side of Equation 19 are available from
261 either the aethalometer or AMS measurements or are otherwise known. It can be seen from Equation 19 that the
262 mass concentrations used to calculate $\mathrm{MAC_{SOA}}$ solely originate from AMS data, thus being consistent with the
263 calculation of $\mathrm{MAC_{POA}}$ (see above). Equation 19 is based on the assumption that POA is "chemically inert", i.e. no
264 chemically induced changes of M_{POA} and $\mathrm{MAC_{POA}}$ occur. Such chemically induced changes of absorption by POA,

if they occur, are assigned to the absorption by SOA, thus resulting in a corresponding adjustment of the inferred MAC_{SOA}.

3.4 Mie calculation to relate k_{OA} with MAC_{OA}

The imaginary part of the refractive index of an aerosol component is an intensive material property. However, the MAC of such an aerosol component additionally depends on the size and morphology of the aerosol (except for the Rayleigh regime). The online aerosol absorption measurements provide estimates for MAC values, while the UV-visible absorbance measurements of filter extracts provide the imaginary part of the refractive index. We used Mie calculations in order to compare the two quantities. The $k_{OA}(\lambda)$obtained from the filter extracts is converted to a $MAC_{OA,bulk}$ by assuming that all OA is present in homogeneous spherical particles with a diameter distribution identical to the mobility diameter distribution measured by the SMPS. In this manner, $MAC_{OA,bulk}$ becomes equal to the mass-weighted average (=volume-weighted average) of the diameter dependent MAC:

$$MAC_{OA,bulk}(\lambda, n_{OA}, k_{OA}, \rho_{OA}) = \frac{\sum_i N_i d_i^3 MAC_i^{Mie}(\lambda, n_{OA}, k_{OA}, \rho_{OA})}{\sum_i N_i d_i^3} \quad (20)$$

Here, N_i and d_i are the number of particles and particle diameter, respectively, in the i^{th} size bin, and n_{OA} is the real part of the refractive index of the OA (which is assumed to be n_{OA} = 1.5 typical for organic material; Lu et al., 2015). The MAC of particles with diameter d_i, MAC_i^{Mie}, was calculated using the Mie Code by Peña and Pal (2009) (incorporated into Igor Pro 6.3, WaveMetrics, OR, USA by Taylor et al., 2015). MAC_i^{Mie} also depends on the density of OA, for which we assume a value of ρ_{OA}= 1.5 g cm^{-3} (see Section 2.2), as the volume specific absorption cross-section obtained from Mie theory needs to be converted to a mass specific absorption cross-section. We note that as we have used the same value of ρ_{OA} in the calculation of both MAC_i^{Mie} and $k_{OA}(\lambda)$, $MAC_{OA,bulk}$ becomes independent of the assumed ρ_{OA} value.

Assuming spherical particles and neglecting the presence of BC in these particles may seem inappropriate. However, calculations considering BC and assuming core-shell morphology revealed (1) limited sensitivity of the resulting MAC_{OA} to this assumption and (2) a higher than measured lensing effect. Therefore, a substantial fraction of the OA seems to be externally mixed and to dominate the measured size distribution (see also Section 4.1). The uncertainty

289 in the MAC_{OA} inferred from k_{OA} of the UV-visible absorbance measurements was estimated by combining an
290 estimated 20 % precision with a detection limit of 0.3 m^2 g^{-1} in quadrature.

291

292 **4. RESULTS AND DISCUSSION**

293 **4.1 Verification of MAC_{BC} and *C* value**

294 As mentioned above, the determination of MAC_{BC}(880nm) requires the determination of the absorption coefficients
295 at λ and the BC mass. We used the aethalometer to obtain the absorption coefficients with high time resolution,
296 while absolute values were scaled to match MWAA data, which we defined as our reference method. The
297 aethalometer was also used to obtain eBC mass concentrations with high time resolution, while absolute values were
298 scaled to match EC mass measured by the Sunset thermo-optical measurement using the EUSAAR-2 protocol,
299 which we defined as our reference method. Here we start by proving the concept of our scaling approaches and
300 provide average values for MAC_{BC}(880nm) and aethalometer-*C* which are required subsequently.

301 Figure 1A shows the correlation between the MWAA measured absorption coefficient at 880 nm and the Sunset
302 thermo-optical EC mass measurements. MWAA absorption measurements at 880 nm is determined by
303 extrapolating the absorption coefficients at 850 nm using an α determined from the ratio between the
304 absorption coefficients at 850 nm and 635nm. The corresponding MAC_{BC}(880nm), determined as the slope of
305 the linear fit through all data, is 4.6 ± 0.7 m^2 g^{-1} . This value matches the data at all three levels of aging, i.e. for the
306 primary, Aged1 and Aged2 filter samples, within experimental uncertainty (see Figure S2 in the Supplement for
307 more information). This average MAC_{BC}(880nm) is also very similar to values reported for "pure" BC (4.7 ± 0.7
308 m^2 g^{-1} at 880 nm) (Bond et al., 2006), indicating no significant lensing effect on absorption by BC from primary or
309 secondary OA. This can also be observed from the time resolved attenuation measurements by the aethalometer at
310 880 nm (Figure S3), suggesting that little (<10%) to no increase in the attenuation coefficients upon SOA formation.
311 If the OA and the BC were internally mixed, the observed variability in the mass fraction of OA (f_{OA}) from 0.1 to
312 0.9 for the fresh and aged samples would result in a high variability in the MAC_{BC}(880nm), with values higher than
313 those reported in the literature, according to Mie calculations assuming core-shell internal mixtures. However, this is
314 not the case. Based on this observation, we conclude that the particles studied are likely not core-shell internal

315 mixtures, although we have measured a mono-modal aerosol population growing during SOA production (Figure
316 S4). An explanation for the occurrence of an external mixture could be that the primary OA and BC particles may
317 have been externally mixed after these species were emitted separately during combustion, preferentially during the
318 pre-ignition and flaming phases, respectively (Corbin et al., 2015a, 2015b; Heringa et al., 2011). These phases may
319 occur consecutively during a burn or simultaneously in different parts of the stove. MAC_{BC}(880nm) found to be
320 constant supports our approach described in Section 2.2 using scaled aethalometer data for BC mass and treating
321 MAC_{BC} at all other wavelengths as a constant across all experiments during the data retrieval process described in
322 Section 3.1.

323 Figure 1B shows the correlation between $b_{\mathrm{ATN,AE33}}$ and $b_{\mathrm{abs,MWAA}}$ measured by the aethalometer and MWAA,
324 respectively. The two variables correlated very well, indicating a constant aethalometer *C*-value, which is the ratio
325 between $b_{\mathrm{ATN,AE33}}$ and $b_{\mathrm{abs,MWAA}}$ (Equation 1), of 3.0±0.3, independent of the type of the aerosol sampled. This is
326 also reflected in the probability density function of individual *C*-values shown in Figure S2 where the standard
327 deviation is found to be as small as $\sigma_C \sim \pm 10\%$. Such constant ratio justifies our approach of applying this single
328 *C* value for all conditions in order to scale the time resolved attenuation measurements by the aethalometer to the
329 MWAA reference method.

330 Note, the manufacturer's default values, which were not applied in our case, are 1.57 for *C* and 12.2 $m^2 g^{-1}$ for
331 σ_{ATN} at 880 nm, which implies an underlying MAC_{BC}(880 nm) of 7.77 $m^2 g^{-1}$ (Gundel et al., 1984 , Drinovec et al.,
332 2015). Therefore, factory default $b_{\mathrm{abs}}(\lambda)$ would have a substantial systematic high bias for the wood combustion
333 aerosols of this study. Meanwhile, the σ_{ATN} calculated at 880 nm, which is the product of the *C* value and MAC_{BC}
334 (Equation 3), is consistent with the manufacturer value of σ_{ATN} (σ_{ATN} values determined here are 15% higher,
335 13.8 $m^2 g^{-1}$ in this study compared to the value of 12.2 $m^2 g^{-1}$ provided by the manufacturer), and the factory default
336 M_{eBC} would agree well with the true M_{BC}, determined here.

337 **4.2 Optical properties of BC, POA, and SOA**

338 In this section we derive the wavelength dependent mass absorption cross-sections for BC, POA and SOA. In Figure
339 2, we display the evolution of $\alpha(370nm, 880nm)$ as a function of OH exposure. Figure 3 shows the relationship
340 between $\alpha(\lambda, 880nm)$ and f_{OA} for primary and aged aerosols.

341 **α of primary emissions.** The $\alpha(370nm, 880nm)$ values computed for the primary aerosol (OH exposure = 0
342 molecules cm^{-3} h) ranged between 1.3 and 1.7 (Figure S5), which is within the range reported previously for
343 biomass-burning emissions (Kirchstetter et al., 2004; Lewis et al., 2008; Zotter et al., 2016). The $\alpha(\lambda, 880nm)$ is
344 close to that of pure BC (~0.9-1.1; Bond et al., 2013; Zotter et al., 2017) for small f_{POA}, while increasing f_{POA}
345 corresponded to a distinct increase of $\alpha(\lambda, 880nm)$. This increase provides clear evidence for the contribution of
346 primary BrC to the absorption at lower wavelengths (shown explicitly in Equation 13). The f_{POA} ranges from 0.23 to
347 0.59, which is lower than f_{POA} reported for open burning emissions (e.g., f_{POA}~0.75, Ulevicius et al (2016)), because
348 our wood-stove emissions feature a more efficient combustion. The systematic decrease in $\alpha(\lambda, 880nm)$ with
349 increasing λ reflects the more-efficient light absorption by BrC at shorter wavelengths (Moosmüller et al., 2011),
350 and shows that the power law wavelength dependence is an inaccurate oversimplification for this mixed aerosol.
351 **Evolution of α with aging.** Figure 3B shows that upon aging, the OA fraction rapidly increased (a typical time
352 series of raw data is shown in Figure S1), reaching an average value of 0.81 (full range for aged OA: 0.74 < f_{OA} <
353 0.89) at high OH exposures (> 2×10^7 molecules cm^{-3} h), and resulting in a corresponding increase of
354 $\alpha_{BC+POA+SOA}(370nm, 880nm)$. The increase of $\alpha_{BC+POA+SOA}(370nm, 880nm)$ and f_{OA} were always correlated
355 and plateaued at OH exposures beyond ~2×10^7 molecules cm^{-3} h, as seen in Figure 2. Also, note in Figure 2 that the
356 highest $\alpha_{BC+POA+SOA}(370nm, 880nm)$ were reached, on average 1.8, during experiments where the f_{OA} was highest.
357 Such strong correlation between SOA formation and $\alpha_{BC+POA+SOA}(370nm, 880nm)$ suggests the production of
358 substantial amounts of brown SOA. A similar relationship is observed between $\alpha_{BC+POA+SOA}(\lambda, 880nm)$ and f_{OA} for
359 higher wavelengths as shown in Figure S6. Similar to the case of POA, a systematic decrease in $\alpha(\lambda, 880nm)$ with
360 increasing λ is observed, reflecting the preferential absorption of BrC SOA at shorter wavelengths. We note that
361 $\alpha_{BC+POA+SOA}(370nm, 880nm)$ as a function of f_{OA} for all experiments lies below the overall trend for the primary
362 aerosol (dashed line in Figure 3B), implying that $MAC_{SOA}(370nm)$ was smaller than $MAC_{POA}(370nm)$.
363 **Determination of MAC_{BC} and MAC_{POA}.** We determined best-fit values for $MAC_{BC}(\lambda)$ and $MAC_{POA}(\lambda)$ from the
364 data shown in Figure 3A. Figure 3A includes least-squares fits of Equation 13 to the data, with $MAC_{BC}(\lambda)$ and
365 $MAC_{POA}(\lambda)$ as fit parameters. The fit results are shown in Table 1. The obtained fit value of $MAC_{BC}(370nm)$ was
366 13.7 m^2 g^{-1} (GSD 1.1), higher but not statistically significantly different from the value suggested by Bond et al.
367 (2013) of 11.1 m^2 g^{-1} with a 95% confidence interval of 3.5 m^2 g^{-1}, considering α_{BC} =1. Meanwhile, the mean
368 $MAC_{POA}(370nm)$ value, equal to 5.5 m^2 g^{-1}, obtained under our conditions for domestic wood burning is ~2.4 times

higher than that obtained by Saleh et al. (2014) for open biomass burning primary emissions, suggesting the presence of more-strongly absorbing organic material under our conditions (this comparison is continued in Section 4.3).

Determination of MAC_{SOA}. The $MAC_{SOA}(\lambda)$ values, determined using Equation 19, are shown in Figure 4 and Table 1. MAC_{SOA}(370nm) was 2.2 m^2 g^{-1} (GSD 1.39), a factor of 2.5 smaller than MAC_{POA}(370nm), but approximately an order of magnitude higher than values reported for ambient oxygenated aerosols or laboratory SOA from biogenic and traditional anthropogenic precursors such as terpenes and methyl-benzenes (Clarke et al., 2007; Lambe et al., 2013; Liu et al., 2016; Romonosky et al., 2015). The predominant SOA precursors identified in wood smoke comprise (methyl)naphthalene(s) and phenol derivatives from lignin pyrolysis (Bruns et al., 2016; Ciarelli et al., 2016), the oxidation products of which are expected to be highly light absorbing due to the presence of aromatic moieties in the SOA (Bruns et al., 2016; Laskin et al., 2015). In this regard, it is not surprising that the MAC_{SOA}(370nm) values obtained here are similarly high as those obtained from methanol-extracted SOA from guaiacol and naphthalene oxidation (0.5–3.0 m^2 g^{-1}, Romonosky et al., 2015).

Uncertainties and variability in MAC_{BC}, MAC_{POA} and MAC_{SOA}. Table 1 shows that the uncertainties in the fitted $MAC_{BC}(\lambda)$ are relatively low (< 10%), increasing with decreasing λ. By contrast, the uncertainties in the fitted MAC_{POA} are much higher (GSD = 1.2–1.5) and increase with increasing λ. The relative residuals between the measured and fitted $\alpha(\lambda, 880\text{nm})$ for primary emissions showed small biases of only 0.07 (Figure S7). The corresponding RMSE (root mean square error) was 0.13, showing that the obtained average values may represent the data well. MAC_{SOA} values determined were highly variable between experiments with a GSD = 1.39 and 2.42 for λ=370 nm and 660 nm, respectively. We expect the variabilities in MAC_{SOA} and of MAC_{POA} to be related to changes in the organic aerosol chemical composition between different burns, since the variability of $MAC_{BC}(\lambda)$ was relatively small. In Section 4.3, we discuss this variability further using the results of an additional and independent analysis.

MAC_{BC}, MAC_{POA} and MAC_{SOA} wavelength dependence. The relationships between the $MAC_{SOA}(\lambda)$, $MAC_{POA}(\lambda)$ and $MAC_{BC}(\lambda)$ and wavelength appear to fall on three unique lines in the range 660 nm to 370 nm when plotted in log-log space, as shown in Figure 4 (Figure S8 shows the same data plotted on a linear scale). This indicates that a power-law approximation provides a good description of the behavior of individual components within this wavelength range from 370 nm to 660 nm. Accordingly we fitted the power law coefficients to the data shown in

Figure 4 ($\ln(\mathrm{MAC}_i) = \ln(\mathrm{A}_i) + \alpha_i \ln(\lambda)$, with i= BC, POA, or SOA) and fitting parameters are shown as multivariate probability density functions in Figure S9. This yielded α_{BC} = 1.2, α_{POA} = 4.6, and α_{SOA} = 5.6. Note that α_{BC} in the range 660 nm to 370 nm obtained from this fit is very similar to α_{BC} values that can be inferred by extrapolating the data shown in Figure 3A to f_{OA}=0. The high α values obtained for the organic fractions are consistent with previous measurements for BrC containing POA (e.g. Chakrabarty et al., 2010, 2013) although, to our knowledge, this is the first study to report α_{SOA} without performing a solvent extraction.

Evolution of $\mathrm{MAC_{OA}}$ with aging. In Figure 5, we examine whether the absorption profile of SOA evolved with aging. A change in $\mathrm{MAC_{SOA}}(370\mathrm{nm})$ or α_{SOA} with increasing OH exposure may indicate either a change in the mass-specific absorption of the condensing SOA species with time, or a change (e.g. "bleaching") in the MAC of pre-existing POA. Figure 5 indicates that neither of these scenarios was the case. Both $\mathrm{MAC_{SOA}}$(370nm) and α_{SOA} were statistically independent of the OH exposure, for exposures up to 40 molec. OH $\mathrm{cm^{-3}}$ h. This signifies that under our conditions and within our measurement uncertainties the optical properties of the additional organic mass formed was constant with aging, under the assumption that the light-absorption properties of POA were negligibly influenced by aging. Most of the variability in $\mathrm{MAC_{SOA}}(\lambda)$ discussed above is therefore related to experiment-to-experiment differences rather than to the extent of OH exposure, as it is also shown below.

4.3 Solubility of BrC in methanol and water

Figure 6 shows the $\mathrm{MAC_{OA}}$(370nm) determined from the water and methanol extracts against the $\mathrm{MAC_{OA}}$(370nm) determined from the online measurements. The $\mathrm{MAC_{OA}}$(370nm) from online measurements was estimated by subtracting the contribution of BC assuming a constant $\mathrm{MAC_{BC}}$(370nm) = 13.7 $\mathrm{m^2.g^{-1}}$ as obtained in this work (Table 1). We performed all the calculations and comparisons at λ = 370 nm, as the signal to noise ratio of the absorption coefficients measured by UV-visible spectroscopy and the contribution of BrC to the total carbonaceous absorption are highest at this wavelength. The MAC of the extracts was computed from the k_{OA} through Mie calculations. Repetition of both water and methanol extracts yielded results that were consistent within 10% (Figure S11). Average raw absorption spectra are shown in Figure S12.

Figure 6B shows excellent correlation between the MAC values obtained from the the k_{OA} of the methanol extracted OA with the in-situ method described above. This correlation suggests that none of the assumptions employed in either method led to substantial errors in precision, providing direct support for our results. A similar relationship

was observed between k_{OA} and the MAC_{OA}(370nm) determined from the online measurements (Figure S13), showing that this relationship is not sensitive to assumptions underlying the Mie calculations. It further suggests that the wide variability observed in the MAC_{OA} values of different burns, as seen Figure 6, most likely reflects real variability in the optical properties of POA and SOA rather than random noise or experimental errors in the retrieved quantities. MAC_{OA} retrieved based on the k_{OA} of the water soluble OA show substantially more scatter than observed in Figure 6B (for both primary and aged data), suggesting a variable extraction efficiency in the case of water, which we also attribute to variability in the OA composition.

The orthogonal, uncertainty-weighted linear regression in Figure 6B shows that the methanol extracts explain 46 ± 10% of the online MAC. (Note that, in this analysis, aged OA refers to the sum of POA and SOA for aged samples.) Considering the simplifying assumptions that were necessary for our Mie analysis and those related to online MAC_{OA} calculations, we consider this an adequate agreement. In particular, the assumption of a perfect extraction efficiency of OA in methanol may have been violated (see Section 3.4). Conversely, the fit in Figure 6A indicates that the apparent MAC of water-soluble species was a fourth of the respective methanol MAC, according to the slope of only 12 ± 3%. . This strong disagreement shows that the BrC in our samples was hardly water soluble, even for the most aged samples. As we expect that the majority of OA in our samples formed by wood pyrolysis (Di Blasi, 2008; Corbin et al., 2015b; Shafizadeh, 1984), we can compare our results directly to those of Chen and Bond (2010), who also found that primary wood-pyrolysis BrC was water insoluble. Moreover, the water-insoluble nature of the light absorbing components of SOA is in line with the results by Bruns et al. (2016) who showed that the precursors of SOA in these experiments were predominantly aromatic compounds.

4.4 Comparison of k_{OA} with literature

The results above highlight the variability in the OA absorption properties. In this section, we discuss potential reasons for this variability and compare our results to literature. Figure 7 shows the imaginary refractive index of methanol-extracted OA at 370 nm, $k_{OA,methanol}$(370nm) (Equation 8), as a function of M_{BC}/M_{OA} and aging. The data are plotted against M_{BC}/M_{OA} instead of f_{OA} to allow for a direct comparison with literature (see Figure S14 for a plot against f_{OA}). An approximately linear trend of $k_{OA,methanol}$(370nm) with M_{BC}/M_{OA} is seen in log space. This aging-independent relationship may be useful in, for example, atmospheric scenarios where wood-burning OA is a dominant aerosol component but its exact degree of aging is unknown. The decrease of M_{BC}/M_{OA} caused by

formation of SOA during aging results in a concurrent decrease of $k_{OA,methanol}$(370nm), implying that $k_{SOA} < k_{POA}$. This result is consistent with the smaller MAC of SOA compared to POA obtained from online measurements (Table 1) and with recent results reported by Sumlin et al. (2017) . We emphasize that the derived quantity here is the imaginary refractive index *k* of the total aged OA, not the SOA.

The increase of $k_{OA,methanol}$(370nm) with increasing M_{BC}/M_{OA} indicates that the OA compounds present at higher M_{BC}/M_{OA} absorbed more efficiently than at low M_{BC}/M_{OA}. If the variability in M_{BC}/M_{OA} was driven partly by OA partitioning, then this implies that lower-volatility compounds were more absorbing than high-volatility compounds, consistent with the results by Saleh et al. (2014) who investigated the relation between OA absorption and volatility using thermodesorber measurements. A correlation between k_{OA} and M_{BC}/M_{OA} has also been reported by Lu et al. (2015). The parameterizations reported by these authors are included in Figure 7, both showing a smaller trend with M_{BC}/M_{OA} than seen in our data. Despite these differences, our results confirm the generality of the correlation proposed by Saleh et al. (2014), but using a method that is independent of potential biases related to internal mixing effects, filter-based absorption measurements or Mie calculations. Indeed, we emphasize that the k_{OA} obtained here is a lower limit: as our approach does not account for the OA extraction efficiency; $k_{OA,methanol}$(370nm) may be underestimated by up to a factor of ~2, based on Figure 6B.

5. ATMOSPHERIC IMPLICATIONS

In this section, we seek to estimate the relative importance of OA absorption at different wavelengths relative to that of the total carbonaceous aerosol as a function of aging. For these calculations, the MAC(λ) values for the different components and their relative mass abundance are required. We used the power law parameters reported above to generate continuous $MAC_{BC}(\lambda)$, $MAC_{POA}(\lambda)$, and $MAC_{SOA}(\lambda)$ functions together with their associated uncertainties (Figure 8A), which allow the extrapolation of these parameters in the range [280nm; 880nm].

The contributions of the different components as a function of OH exposure were calculated by assuming that SOA production follows the first order decay of its precursors, i.e., the reaction with OH. Under this assumption, the time-dependent mass concentration of SOA compared to POA can be expressed as

$$M_{SOA,WLC}(t)/M_{POA,WLC}(t) = M_{SOAP,WLC}/M_{POA,WLC} \times \left(1 - \exp\left(-k_{OH} OH_{exp}\right)\right) \quad (21)$$

In this equation, $M_{\mathrm{SOA,WLC}}(t)$, $M_{\mathrm{POA,WLC}}(t)$ and $M_{\mathrm{SOAP,WLC}}$ are the wall loss corrected mass concentrations of SOA, POA and the SOA potential (the maximum SOA formed upon the consumption of all precursors). k_{OH} represents an estimation of reaction rate of SOA precursors towards OH based on SOA production rates. By fitting the observed $M_{\mathrm{SOA,WLC}}(t)/M_{\mathrm{POA,WLC}}(t)$ against the OH exposure, k_{OH} and $M_{\mathrm{SOAP,WLC}}/M_{\mathrm{POA,WLC}}$ can be estimated. For these calculations, we have estimated the wall losses using two approaches as described in the SI.

The $M_{\mathrm{SOAP,WLC}}/M_{\mathrm{POA,WLC}}$ was on average equal to 7.8 (GSD = 1.4) and k_{OH} was estimated as 2.7×10^{-11} molecule^{-1} cm^3 (GSD = 1.4), consistent with the chemically speciated data obtained by a proton-transfer-reaction mass spectrometer (PTR-MS) (Bruns et al., 2016, 2017). These high rates and enhancement ratios indicate the rapid production of SOA. Based on the bulk gas phase measurements of SOA precursors (Bruns et al., 2016), the obtained enhancements are consistent with high bulk SOA yields of ~50%. These high values are not surprising, considering the nature of these gases (e.g. PAH and phenol derivatives), the low temperatures (263 K), and the relatively high concentrations (Aged OA ~100 µg m^{-3}) at which the experiments have been conducted (Bruns et al. 2016).

Combining these calculated enhancements with the average contributions of POA in primary emissions, the evolution of f_{OA} with aging was determined and is shown in Figure 8B. The uncertainties in Figure 8B (dotted lines) represent one standard deviation on f_{OA} obtained by a Monte Carlo propagation of uncertainties due to experiment-to-experiment variability, fitting errors and wall loss correction errors (see SI). While this calculation represents a simplification of the SOA production mechanisms (the dependence of SOA yields on OH exposures/multigeneration chemistry and OA mass concentrations was neglected), it results in residuals much smaller than the experiment-to-experiment variability. We therefore used these calculations to assess the relative contribution of OA to the total carbonaceous absorption. We show in Figure 8C that below 400 nm and upon aging, the absorption coefficient of the total organics was at least as high as the one of BC.

Using the MAC values of the different components (in m^2 g^{-1}), their abundance (in g m^{-3}) and the solar irradiance data (S, in W m^{-2} nm^{-1}) calculated at sea level for a cloudless day, the fractional energy transfer due to the BrC light absorption relative to that due to the total carbonaceous aerosol absorption , $W_{\mathrm{OA}}(OH_{\mathrm{exp}})$, in air masses dominated by residential burning emissions can be determined as

$$W_{\mathrm{OA}}(OH_{\mathrm{exp}}) = RET_{\mathrm{OA}}(OH_{\mathrm{exp}})/RET_{\mathrm{tot}}(OH_{\mathrm{exp}})$$

$$= \frac{\int_{300}^{880}\{M_{\mathrm{POA}}(OH_{\mathrm{exp}})\times MAC_{\mathrm{POA}}(\lambda)+M_{\mathrm{SOA}}(OH_{\mathrm{exp}})\times MAC_{\mathrm{SOA}}(\lambda)\}\times S(\lambda)\times d\lambda}{\int_{300}^{880}\{M_{\mathrm{BC}}(OH_{\mathrm{exp}})\times MAC_{\mathrm{BC}}(\lambda)+M_{\mathrm{POA}}(OH_{\mathrm{exp}})\times MAC_{\mathrm{POA}}(\lambda)+M_{\mathrm{SOA}}(OH_{\mathrm{exp}})\times MAC_{\mathrm{SOA}}(\lambda)\}\times S(\lambda)\times d\lambda} \quad (22)$$

Here, $RET_{\mathrm{OA}}(OH_{\mathrm{exp}})$ and $RET_{\mathrm{tot}}(OH_{\mathrm{exp}})$ denote the rate of energy transfer per volume (in W m^{-3}) to the air mass in question due to light absorption by OA and the total carbonaceous aerosol, respectively. We note that while $RET_{\mathrm{OA}}(OH_{\mathrm{exp}})$ and $RET_{\mathrm{tot}}(OH_{\mathrm{exp}})$ are extensive properties, $W_{\mathrm{OA}}(OH_{\mathrm{exp}})$ does not depend on the loading or scattering/lensing, provided that scattering/lensing similarly affects BC and OA present in the same air mass (e.g. BC and OA have a similar size distribution).

We also note that $W_{\mathrm{OA}}(OH_{\mathrm{exp}})$ depends on the photon flux, $S(\lambda)$, but we consider this dependence to be trivial compared to the variability in the aerosol emissions and their light absorbing properties (error bars considering these variabilities are shown in Figure 8D). Errors in W_{OA} were propagated by Monte Carlo simulations using the uncertainties from the estimated MAC values of BC and OA fractions and the variability in f_{OA}. Our error analysis suggests that the major part of the variance in predicting W_{OA} for primary emissions stems from the variability in the POA mass fraction. In contrast, the SOA mass absorption cross-sections at lower wavelengths are the most critical factor for assessing the relative importance of BrC absorptivity in aged emissions.

Figure 8D shows that the fractional energy transfer to the air mass, W_{OA}, due to the absorption by the primary organic aerosol was around 10% of that of the total carbonaceous aerosol for our samples. This percentage is comparable to that observed by Fu et al. (2012), in spite of f_{OA} in their samples being much higher, because of the high OA MACs in our samples (Table 1). Moreover, with aging, the fraction of OA is enhanced, resulting in a sizeable increase W_{OA}, from ~0.1 to ~0.3 (Figure 8D), highlighting that SOA formation in biomass burning plumes is an atmospherically relevant source of BrC. We note that our data are more representative of flaming conditions. More data are needed on the chemical nature of primary particulate emissions and of the contributing SOA precursors as well as the absorptivity of these primary and secondary products, for better constraining the influence of biomass-burning related BrC on the Earth's climate.

6. CONCLUSIONS

We determined wavelength-dependent MAC values of BC, POA and SOA, as well as k_{OA} for methanol and water extracts of fresh and aged OA, for wood-burning emissions through smog-chamber experiments. To our knowledge, this is the first determination of these properties for wood-burning OA. We showed that the $\mathrm{MAC_{OA}}$(370nm) values

530 calculated based on k_{OA} through Mie analysis correlated well with those estimated from online filter based
531 measurements. This correlation between independent MAC measurements supports the quality of both methods.
532 While MAC_{OA}(370nm) values computed based on $k_{OA,methanol}$ were a 2-fold lower than those estimated from online
533 filter based measurements, calculations based on $k_{OA,water}$ could only explain 12% of the measured absorption,
534 suggesting that BrC species in POA and SOA are mostly water insoluble. The MAC_{OA} was found to vary by more
535 than one order of magnitude. Similar to previous reports, this variability could be related to the variability in the
536 ratio of the mass concentrations of BC and OA (M_{BC}/M_{OA}) due to very different mechanisms of oxidative aging and
537 burn-to-burn variability.

538 The MAC_{POA} and MAC_{SOA} determined for wavelengths between 370 and 660 nm followed a power-law dependence
539 on λ with an absorption Ångström exponent of 4.6 and 5.6 for POA and SOA, respectively. In addition to following
540 this power law, the MACs of POA and SOA appeared to be constant for OH exposures up to 40 x 10^6 molecules cm^{-3} h.

542 The mean MAC_{POA}(370nm) obtained under our conditions was 5.5 $m^2 g^{-1}$, considerably higher than previously
543 reported values for open biomass burning. The mean MAC_{SOA}(370nm) was 2.4 $m^2 g^{-1}$ under our experimental
544 conditions, 2.3 times lower than the mean MAC_{POA}(370nm) but approximately an order of magnitude higher than
545 MAC values estimated for ambient oxygenated aerosols or reported for SOA from biogenic and traditional
546 anthropogenic precursors. We propose that the important role of oxidized phenols and aromatics in forming wood-
547 burning SOA (Bruns et al., 2016) is the cause of this observation. This hypothesis is supported by our observed
548 reaction rates with OH, and by the water-insolubility of the BrC in aged OA.

549 Overall, the absorption by organic aerosols was estimated to contribute 10-30% of the total solar absorption of
550 wood-combustion aerosols, where 10% represents the primary OA and 30% the aged OA. SOA formation in
551 biomass burning plumes is therefore an atmospherically relevant source of BrC.

552 *Acknowledgements.* The research leading to these results has received funding from the European Research Council
553 grant (ERC-CoG 615922-BLACARAT) and by the Competence Centre Energy and Mobility (CCEM) project 807.

554

555

556

References

Alexander, D. T. L., Crozier, P. A. and Anderson, J. R.: Brown carbon spheres in East Asian outflow and their optical properties., Science, 321(5890), 833–6, doi:10.1126/science.1155296, 2008.

Andreae, M. O. and Gelencsér, A.: Black carbon or brown carbon? the nature of light-absorbing carbonaceous aerosols, Atmos. Chem. Phys., 6(3), 3419–3463, doi:10.5194/acpd-6-3419-2006, 2006.

Barmet, P., Dommen, J., DeCarlo, P. F., Tritscher, T., Praplan, A. P., Platt, S. M., Prévôt, A. S. H., Donahue, N. M. and Baltensperger, U.: OH clock determination by proton transfer reaction mass spectrometry at an environmental chamber, Atmos. Meas. Tech., 5(3), 647–656, doi:10.5194/amt-5-647-2012, 2012.

Bertrand, A., Stefenelli, G., Bruns, E. A., Pieber, S. M., Pr, S. H., Wortham, H., Temime-roussel, B., Slowik, J. G., Haddad, I. El and Marchand, N.: Primary emissions and secondary aerosol production potential from woodstoves for residential heating : influence of the stove technology and combustion efficiency, Atmos. Environ., 169, doi:10.1016/j.atmosenv.2017.09.005, 2017.

Di Blasi, C.: Modeling chemical and physical processes of wood and biomass pyrolysis, Prog. Energy Combust. Sci., 34(1), 47–90, doi:10.1016/j.pecs.2006.12.001, 2008.

Bond, T. C., Habib, G. and Bergstrom, R. W.: Limitations in the enhancement of visible light absorption due to mixing state, J. Geophys. Res. Atmos., 111(20), 1–13, doi:10.1029/2006JD007315, 2006.

Bond, T. C., Doherty, S. J., Fahey, D. W., Forster, P. M., Berntsen, T., Deangelo, B. J., Flanner, M. G., Ghan, S., Kärcher, B., Koch, D., Kinne, S., Kondo, Y., Quinn, P. K., Sarofim, M. C., Schultz, M. G., Schulz, M., Venkataraman, C., Zhang, H., Zhang, S., Bellouin, N., Guttikunda, S. K., Hopke, P. K., Jacobson, M. Z., Kaiser, J. W., Klimont, Z., Lohmann, U., Schwarz, J. P., Shindell, D., Storelvmo, T., Warren, S. G. and Zender, C. S.: Bounding the role of black carbon in the climate system: a scientific assessment, J. Geophys. Res. Atmos., 118(11), 5380–5552, doi:10.1002/jgrd.50171, 2013.

Bruns, E. A., Krapf, M., Orasche, J., Huang, Y., Zimmermann, R., Drinovec, L., Močnik, G., El-Haddad, I., Slowik, J. G., Dommen, J., Baltensperger, U. and Prévôt, A. S. H.: Characterization of primary and secondary wood combustion products generated under different burner loads, Atmos. Chem. Phys., 15(5), 2825–2841, doi:10.5194/acp-15-2825-2015, 2015.

Bruns, E. A., El Haddad, I., Slowik, J. G., Kilic, D., Klein, F., Baltensperger, U. and Prévôt, A. S. H.: Identification of significant precursor gases of secondary organic aerosols from residential wood combustion., Sci. Rep., 6, 27881, doi:10.1038/srep27881, 2016.

Bruns, E. A., Slowik, J. G., Haddad, I. El, Kilic, D., Klein, F. and Dommen, J.: Characterization of gas-phase organics using proton transfer reaction time-of-flight mass spectrometry : fresh and aged residential wood combustion emissions, Atmos. Chem. Phys., 705–720, doi:10.5194/acp-17-705-2017, 2017.

Cavalli, F., Viana, M., Yttri, K. E., Genberg, J. and Putaud, J.-P.: Toward a standardised thermal-optical protocol for measuring atmospheric organic and elemental carbon: the EUSAAR protocol, Atmos. Meas. Tech., 3(1), 79–89, doi:doi:10.5194/amt-3-79-2010, 2010.

Chakrabarty, R. K., Moosmüller, H., Chen, L. W. A., Lewis, K., Arnott, W. P., Mazzoleni, C., Dubey, M. K., Wold, C. E., Hao, W. M. and Kreidenweis, S. M.: Brown carbon in tar balls from smoldering biomass combustion, Atmos. Chem. Phys., 10(13), 6363–6370, doi:10.5194/acp-10-6363-2010, 2010.

Chakrabarty, R. K., Arnold, I. J., Francisco, D. M., Hatchett, B., Hosseinpour, F., Loria, M., Pokharel, A. and Woody, B. M.: Black and brown carbon fractal aggregates from combustion of two fuels widely used in asian rituals, J. Quant. Spectrosc. Radiat. Transf., 122, 25–30, doi:10.1016/j.jqsrt.2012.12.011, 2013.

Chen, Y. and Bond, T. C.: Light absorption by organic carbon from wood combustion, Atmos. Chem. Phys., 10, 1773-1787, doi:10.5194/acp-10-1773-2010, 2010.

600 Ciarelli, G., Haddad, I. El, Bruns, E. and Aksoyoglu, S.: Constraining a hybrid volatility basis set model for aging of
601 wood burning emissions using smog chamber experiments, Geosci. Model. Dev., 2303-2320, doi:10.5194/gmd-
602 2303-2017, 2017.

603 Clarke, A., McNaughton, C., Kapustin, V., Shinozuka, Y., Howell, S., Dibb, J., Zhou, J., Anderson, B. E.,
604 Brekhovskikh, V., Turner, H. and Pinkerton, M.: Biomass burning and pollution aerosol over North America:
605 organic components and their influence on spectral optical properties and humidification response, J. Geophys. Res.
606 Atmos., 112(12), 1–13, doi:10.1029/2006JD007777, 2007.

607 Corbin, J. C., Lohmann, U., Sierau, B., Keller, A., Burtscher, H. and Mensah, A. A.: Black carbon surface oxidation
608 and organic composition of beech-wood soot aerosols, Atmos. Chem. Phys., 15(20), 11885–11907, doi:10.5194/acp-
609 15-11885-2015, 2015a.

610 Corbin, J. C., Keller, A., Lohmann, U., Burtscher, H., Sierau, B. and Mensah, A. A.: Organic emissions from a wood
611 stove and a pellet stove before and after simulated atmospheric aging, Aerosol Sci. Technol., 49(11), 1037–1050,
612 doi:10.1080/02786826.2015.1079586, 2015b.

613 DeCarlo, P. F., Kimmel, J. R., Trimborn, A., Northway, M. J., Jayne, J. T., Aiken, A. C., Gonin, M., Fuhrer, K.,
614 Horvath, T., Docherty, K. S., Worsnop, D. R. and Jimenez, J. L.: Field deployable, high resolution, time-of-flight
615 aerosol mass spectrometer, Anal. Chem., 78(24), 8281–8289, doi:8410.1029/2001JD001213.Analytical, 2006.

616 Denier Van Der Gon, H. A. C., Bergström, R., Fountoukis, C., Johansson, C., Pandis, S. N., Simpson, D. and
617 Visschedijk, A. J. H.: Particulate emissions from residential wood combustion in Europe - revised estimates and an
618 evaluation, Atmos. Chem. Phys., 15(11), 6503–6519, doi:10.5194/acp-15-6503-2015, 2015.

619 Drinovec, L., Močnik, G., Zotter, P., Prévôt, A. S. H., Ruckstuhl, C., Coz, E., Rupakheti, M., Sciare, J., Müller, T.,
620 Wiedensohler, A. and Hansen, A. D. A.: The "dual-spot" aethalometer: an improved measurement of aerosol black
621 carbon with real-time loading compensation, Atmos. Meas. Tech., 8(5), 1965–1979, doi:10.5194/amt-8-1965-2015,
622 2015.

623 Feng, Y., Ramanathan, V. and Kotamarthi, V. R.: Brown carbon: a significant atmospheric absorber of solar
624 radiation, Atmos. Chem. Phys., 13(17), 8607–8621, doi:10.5194/acp-13-8607-2013, 2013.

625 Fu, J. S., Hsu, N. C., Gao, Y., Huang, K., Li, C., Lin, N. H. and Tsay, S. C.: Evaluating the influences of biomass
626 burning during 2006 BASE-ASIA: a regional chemical transport modeling, Atmos. Chem. Phys., 12(9), 3837–3855,
627 doi:10.5194/acp-12-3837-2012, 2012.

628 Grieshop, A. P., Logue, J. M., Donahue, N. M. and Robinson, A. L.: Laboratory investigation of photochemical
629 oxidation of organic aerosol from wood fires – part 1: measurement and simulation of organic aerosol evolution,
630 Atmos. Chem. Phys., 9, 2227–2240, doi:10.5194/acp-9-2227-2009, 2009.

631 Gundel, L. A., Dod, R. L., Rosen, H. and Novakov.: The relationship between optical attenuation and black carbon
632 concentration for ambient and source particles, Sci. Total Environ., 36, 197-202, 1984.

633 Hecobian, A., Zhang, X., Zheng, M., Frank, N., Edgerton, E. S. and Weber, R. J.: Water-soluble organic aerosol
634 material and the light-absorption characteristics of aqueous extracts measured over the southeastern United States,
635 Atmos. Chem. Phys., 10(13), 5965–5977, doi:10.5194/acp-10-5965-2010, 2010.

636 Heringa, M. F., DeCarlo, P. F., Chirico, R., Tritscher, T., Dommen, J., Weingartner, E., Richter, R., Wehrle, G.,
637 Prévôt, A. S. H. and Baltensperger, U.: Investigations of primary and secondary particulate matter of different wood
638 combustion appliances with a high-resolution time-of-flight aerosol mass spectrometer, Atmos. Chem. Phys.,
639 11(12), 5945–5957, doi:10.5194/acp-11-5945-2011, 2011.

640 Hoffer, A., Gelencsér, A., Guyon, P., Kiss, G., Schmid, O., Frank, G. P., Artaxo, P. and Andreae, M. O.: Optical
641 properties of humic-like substances (HULIS) in biomass-burning aerosols, Atmos. Chem. Phys., 6, 3563-3570,
642 doi:10.5194/acp-6-3563-2006, 2006.

643 Jo, D. S., Park, R. J., Lee, S., Kim, S. W. and Zhang, X.: A global simulation of brown carbon: Implications for

photochemistry and direct radiative effect, Atmos. Chem. Phys., 16(5), 3413–3432, doi:10.5194/acp-16-3413-2016, 2016.

Kirchstetter, T. W., Novakov, T. and Hobbs, P. V.: Evidence that the spectral dependence of light absorption by aerosols is affected by organic carbon, J. Geophys. Res. D Atmos., 109(21), 1–12, doi:10.1029/2004JD004999, 2004.

Krapf, M., Haddad, I. El, Bruns, E. A., Krapf, M., Haddad, I. El, Bruns, E. A., Molteni, U. and Daellenbach, K. R.: Labile peroxides in secondary organic aerosol labile peroxides in secondary organic aerosol, Chem 1, 603–616, doi:10.1016/j.chempr.2016.09.007, 2016.

Lack, D. A. and Langridge, J. M.: On the attribution of black and brown carbon light absorption using the Ångström exponent, Atmos. Chem. Phys., 13(20), 10535–10543, doi:10.5194/acp-13-10535-2013, 2013.

Lambe, A. T., Cappa, C. D., Massoli, P., Onasch, T. B., Forestieri, S. D., Martin, A. T., Cummings, M. J., Croasdale, D. R., Brune, W. H., Worsnop, D. R. and Davidovits, P.: Relationship between oxidation level and optical properties of secondary organic aerosol, Environ. Sci. Technol., 47(12), 6349–6357, doi:10.1021/es401043j, 2013.

Laskin, A., Laskin, J. and Nizkorodov, S. A.: Chemistry of atmospheric brown carbon, Chem. Rev., 115(10), 4335–4382, doi:10.1021/cr5006167, 2015.

Lee, H. J., Aiona, P. K., Laskin, A., Laskin, J. and Nizkorodov, S. A.: Effect of solar radiation on the optical properties and molecular composition of laboratory proxies of atmospheric brown carbon, Environ. Sci. Technol., 48(17), 10217–10226, doi:10.1021/es502515r, 2014.

Lewis, K., Arnott, W. P., Moosmüller, H. and Wold, C. E.: Strong spectral variation of biomass smoke light absorption and single scattering albedo observed with a novel dual-wavelength photoacoustic instrument, J. Geophys. Res. Atmos., 113(16), 1–14, doi:10.1029/2007JD009699, 2008.

Lin, G., Penner, J. E., Flanner, M. G., Sillman, S., Xu, L. and Zhou, C.: Radiative forcing of organic aerosol in the atmosphere and on snow: effect of SOA and brown carbon, J. Geophys. Res. - Atmos., 119(12), 7453–7476, doi:10.1002/2013JD021186.Received, 2014.

Liu, J., Scheuer, E., Dibb, J., Ziemba, L. D., Thornhill, K. L., Anderson, B. E., Wisthaler, A., Mikoviny, T., Devi, J. J., Bergin, M. and Weber, R. J.: Brown carbon in the continental troposphere, Geophys. Res. Lett., 41, 2191–2195, doi:10.1002/2013GL058976, 2014.

Liu, J., Lin, P., Laskin, A., Laskin, J., Kathmann, S. M., Wise, M., Caylor, R., Imholt, F., Selimovic, V. and Shilling, J. E.: Optical properties and aging of light absorbing secondary organic aerosol, Atmos. Chem. Phys., 16, 12815-12827, doi:10.5194/acp-2016-482, 2016.

Liu, P. F., Abdelmalki, N., Hung, H. M., Wang, Y., Brune, W. H. and Martin, S. T.: Ultraviolet and visible complex refractive indices of secondary organic material produced by photooxidation of the aromatic compounds toluene and m-xylene, Atmos. Chem. Phys., 15(3), 1435–1446, doi:10.5194/acp-15-1435-2015, 2015a.

Liu, S., Aiken, A. C., Gorkowski, K., Dubey, M. K., Cappa, C. D., Williams, L. R., Herndon, S. C., Massoli, P., Fortner, E. C., Chhabra, P. S., Brooks, W. A., Onasch, T. B., Jayne, J. T., Worsnop, D. R., China, S., Sharma, N., Mazzoleni, C., Xu, L., Ng, N. L., Liu, D., Allan, J. D., Lee, J. D., Fleming, Z. L., Mohr, C., Zotter, P., Szidat, S. and Prévôt, A. S. H.: Enhanced light absorption by mixed source black and brown carbon particles in UK winter, Nat. Commun., 8435, doi:10.1038/ncomms9435, 2015b.

Lu, Z., Streets, D. G., Winijkul, E., Yan, F., Chen, Y., Bond, T. C., Feng, Y., Dubey, M. K., Liu, S., Pinto, J. P. and Carmichael, G. R.: Light absorption properties and radiative effects of primary organic aerosol emissions, Environ. Sci. Technol., 49, 4868–4877, doi:10.1021/acs.est.5b00211, 2015.

Massabò, D., Caponi, L., Bernardoni, V., Bove, M. C., Brotto, P., Calzolai, G., Cassola, F., Chiari, M., Fedi, M. E., Fermo, P., Giannoni, M., Lucarelli, F., Nava, S., Piazzalunga, A., Valli, G., Vecchi, R. and Prati, P.: Multi-

688 wavelength optical determination of black and brown carbon in atmospheric aerosols, Atmos. Environ., 108, 1–12,
689 doi:10.1016/j.atmosenv.2015.02.058, 2015.

690 Massabò, D., Bernardoni, V., Bove, M. C., Brunengo, A., Cuccia, E., Piazzalunga, A., Prati, P., Valli, G. and
691 Vecchi, R.: A multi-wavelength optical set-up for the characterization of carbonaceous particulate matter, J. Aerosol
692 Sci., 60, 34–46, doi:10.1016/j.jaerosci.2013.02.006, 2013.

693 Moosmüller, H., Chakrabarty, R. K. and Arnott, W. P.: Aerosol light absorption and its measurement: A review, J.
694 Quant. Spectrosc. Radiat. Transf., 110(11), 844–878, doi:10.1016/j.jqsrt.2009.02.035, 2009.

695 Moosmüller, H., Chakrabarty, R. K., Ehlers, K. M. and Arnott, W. P.: Absorption Ångström coefficient, brown
696 carbon, and aerosols: Basic concepts, bulk matter, and spherical particles, Atmos. Chem. Phys., 11(3), 1217–1225,
697 doi:10.5194/acp-11-1217-2011, 2011.

698 Petzold, A. and Schönlinner, M.: Multi-angle absorption photometry - A new method for the measurement of
699 aerosol light absorption and atmospheric black carbon, J. Aerosol Sci., 35(4), 421–441,
700 doi:10.1016/j.jaerosci.2003.09.005, 2004.

701 Platt, S. M., El Haddad, I., Zardini, A. A., Clairotte, M., Astorga, C., Wolf, R., Slowik, J. G., Temime-Roussel, B.,
702 Marchand, N., Ježek, I., Drinovec, L., Močnik, G., Möhler, O., Richter, R., Barmet, P., Bianchi, F., Baltensperger,
703 U. and Prévôt, A. S. H.: Secondary organic aerosol formation from gasoline vehicle emissions in a new mobile
704 environmental reaction chamber, Atmos. Chem. Phys., 13(18), 9141–9158, doi:10.5194/acp-13-9141-2013, 2013.

705 Romonosky, D. E., Laskin, A., Laskin, J. and Nizkorodov, S. A.: High-resolution mass spectrometry and molecular
706 characterization of aqueous photochemistry products of common types of secondary organic aerosols, J. Phys.
707 Chem. A, 119(11), 2594–2606, doi:10.1021/jp509476r, 2015.

708 Saleh, R., Hennigan, C. J., McMeeking, G. R., Chuang, W. K., Robinson, E. S., Coe, H., Donahue, N. M. and
709 Robinson, A. L.: Absorptivity of brown carbon in fresh and photo-chemically aged biomass-burning emissions,
710 Atmos. Chem. Phys., 13(15), 7683–7693, doi:10.5194/acp-13-7683-2013, 2013.

711 Shafizadeh, F.: The chemistry of pyrolysis and combustion. The chemistry of solid Wood, ACS Symp. Ser., 207,
712 489–529, doi:10.1021/ba-1984-0207.ch013\r10.1021/ba-1984-0207.ch013, 1984.

713 Sumlin, B. J., Pandey, A., Walker, M. J., Pattison, R. S., Williams, B. J., and Chakrabarty, R. K.: Atmospheric
714 photooxidation diminishes light absorption by primary brown carbon aerosol from biomass burning, Environ. Sci.
715 Technol. Lett., 4(12), 540-545, doi:10.1021/acs.estlett.7b00393, 2017.

716 Sun, H., Biedermann, L. and Bond, T. C.: Color of brown carbon: A model for ultraviolet and visible light
717 absorption by organic carbon aerosol, Geophys. Res. Lett., 34(17), 1–5, doi:10.1029/2007GL029797, 2007.

718 Ulevicius, V., Bozzetti, C., Vlachou, A., Plauškait, K., Mordas, G., Dudoitis, V., Abbaszade, G., Remeikis, V.,
719 Garbaras, A., Masalaite, A., Blees, J., Fröhlich, R., Dällenbach, K. R., Canonaco, F., Slowik, J. G., Dommen, J.,
720 Zimmermann, R., Schnelle-kreis, J., Salazar, G. A. and Agrios, K.: Fossil and non-fossil source contributions to
721 atmospheric carbonaceous aerosols during extreme spring grassland fires in Eastern Europe, Atmos. Chem. Phys.,
722 16, 5513–5529, doi:10.5194/acp-16-5513-2016, 2016.

723 Wang, X., Heald, C. L., Ridley, D. A., Schwarz, J. P., Spackman, J. R., Perring, A. E., Coe, H., Liu, D. and Clarke,
724 A. D.: Exploiting simultaneous observational constraints on mass and absorption to estimate the global direct
725 radiative forcing of black carbon and brown carbon, Atmos. Chem. Phys., 14(20), 10989–11010, doi:10.5194/acp-
726 14-10989-2014, 2014.

727 Weingartner, E., Saathoff, H., Schnaiter, M., Streit, N., Bitnar, B. and Baltensperger, U.: Absorption of light by soot
728 particles: determination of the absorption coefficient by means of aethalometers, J. Aerosol Sci., 34(10), 1445–1463,
729 doi:10.1016/S0021-8502(03)00359-8, 2003.

730 Zhao, R., Lee, A. K. Y., Huang, L., Li, X., Yang, F. and Abbatt, J. P. D.: Photochemical processing of aqueous
731 atmospheric brown carbon, Atmos. Chem. Phys., 15(11), 6087–6100, doi:10.5194/acp-15-6087-2015, 2015.

732 Zotter, P., Herich, H., Gysel, M., El-Haddad, I., Zhang, Y., Močnik, G., Hüglin, C., Baltensperger, U., Szidat, S. and
733 Prévôt, A. S. H.: Evaluation of the absorption Ångström exponents for traffic and wood burning in the Aethalometer
734 based source apportionment using radiocarbon measurements of ambient aerosol, Atmos. Chem. Phys., 17, 4229-
735 4249, doi:10.5194/acp-17-4229-2017, 2017.

736 Zotter, P., Herich, H., Gysel, M., El-haddad, I., Zhang, Y. and Moˇ, G.: Evaluation of the absorption Ångström
737 exponents for traffic and wood burning in the Aethalometer-based source apportionment using radiocarbon
738 measurements of ambient aerosol, , 4229–4249, doi:10.5194/acp-17-4229-2017, 2017.

739
740
741
742
743
744
745
746
747
748
749
750
751
752
753
754
755
756
757
758
759
760
761
762
763

Atmos. Chem. Phys. Discuss., https://doi.org/10.5194/acp-2018-159
Manuscript under review for journal Atmos. Chem. Phys.
Discussion started: 13 April 2018

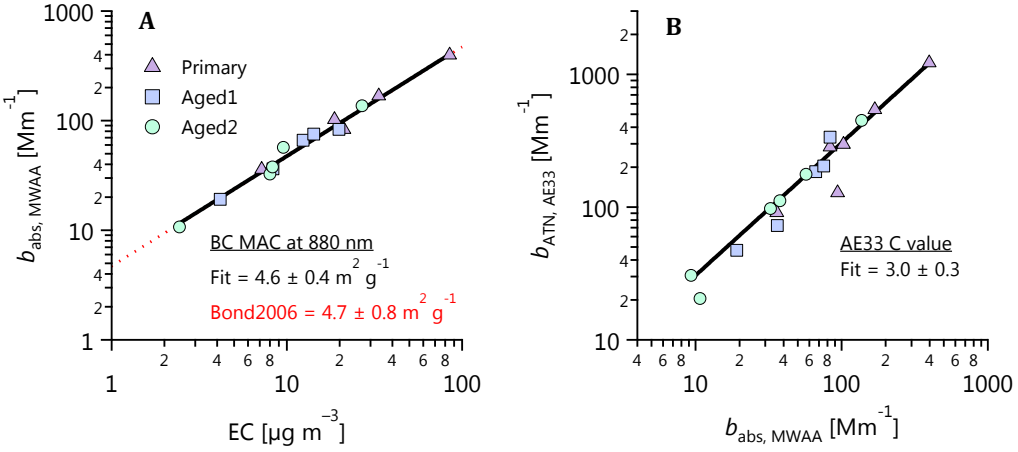

Figure 1: Determination of (A) MAC_{BC}(880nm) and (B) aethalometer *C* value using MWAA absorption measurements, thermal/optical EC (EUSAAR2 protocol) and aethalometer attenuation measurements. MWAA absorption measurements at 880 nm is determined by extrapolating the absorption coefficients at 850 nm using an α determined from the ratio between the absorption coefficients at 850 nm and 635nm. The aerosols were either primary (no OH exposure), Aged 1 (~1x10⁷ molec OH cm⁻³ h), or Aged 2 (~4x10⁷ molec OH cm⁻³ h). No difference in MAC or *C* value was discernable with aging (see also Figure S2). Also shown is the MAC of pure BC recommended by Bond et al. (2006) (dotted line in A). The *C* value derived from σ_{ATN} recommended by Drinovec et al. (2015) = 2.6 compares well with the value derived in Figure 1B.

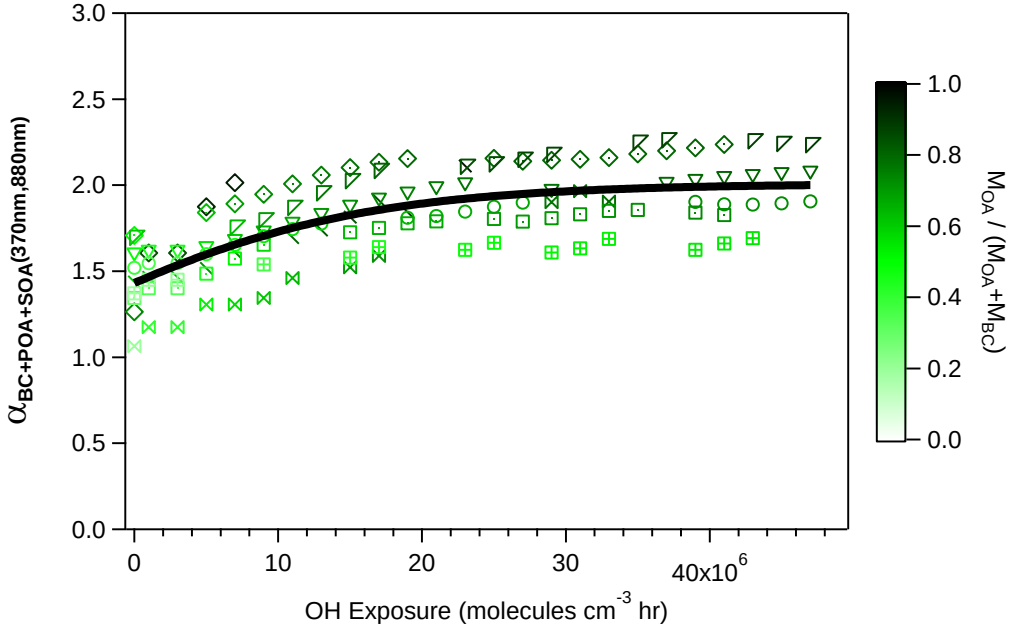

Figure 2: Evolution during photochemical aging of $\alpha_{BC+POA+SOA}(370nm, 880nm)$ (two-wavelength Ångström exponent calculated using total absorption data at 370 nm and 880 nm), where the different symbols denote individual experiments. Data are colored by the OA mass fraction $f_{OA} = M_{OA}/(M_{OA} + M_{BC})$. The black line is a fit to guide the eye.

Atmos. Chem. Phys. Discuss., https://doi.org/10.5194/acp-2018-159
Manuscript under review for journal Atmos. Chem. Phys.
Discussion started: 13 April 2018

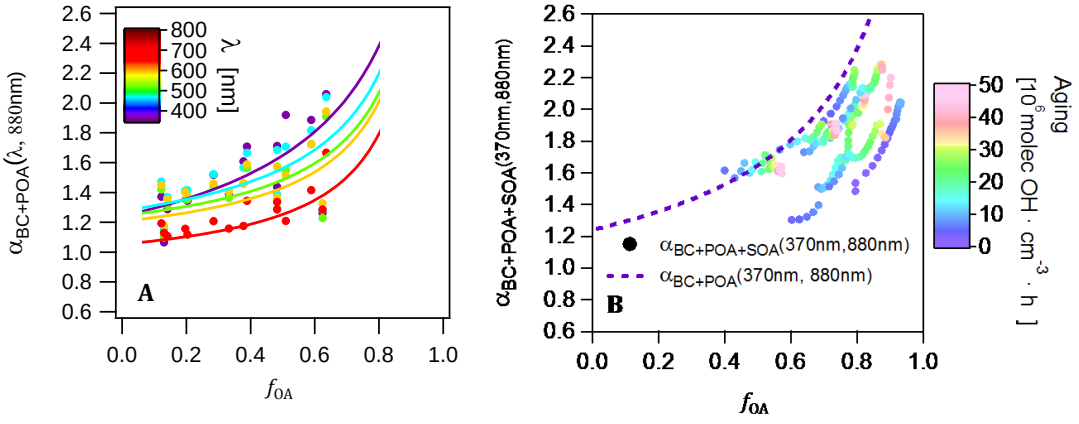

Figure 3: (A) Relationship of $\alpha_{BC+POA}(\lambda, 880nm)$ to f_{OA} for seven wavelengths. Lines are fits of Equation 13 to the data. (B) Relationship of $\alpha_{BC+POA+SOA}(370nm, 880nm)$ to f_{OA} for several experiments. Data in (A) and (B) are colored by the wavelength and OH exposure, respectively.

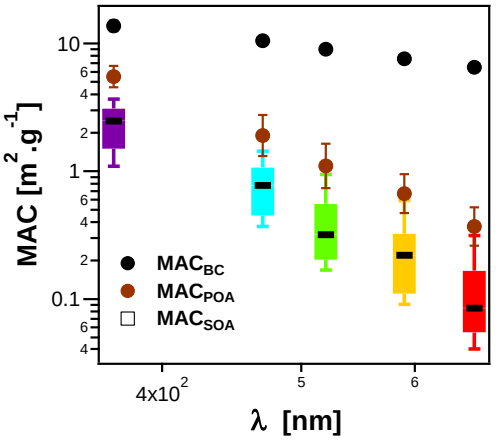

Figure 4: $MAC_{SOA}(\lambda)$ calculated from several smog chamber experiments plotted as box-whiskers as a function of wavelength (also shown by the color of the bars). The thick black lines, the boxes and the whiskers mark the medians, the quartiles and the 10th and the 90th percentiles, respectively. Also shown are the $MAC_{BC}(\lambda)$ and $MAC_{POA}(\lambda)$ reported in Table 1. Note that $MAC_{SOA}(880nm)$ and $MAC_{POA}(880nm)$ are zero by definition.

Atmos. Chem. Phys. Discuss., https://doi.org/10.5194/acp-2018-159
Manuscript under review for journal Atmos. Chem. Phys.
Discussion started: 13 April 2018

Atmospheric Chemistry and Physics Discussions

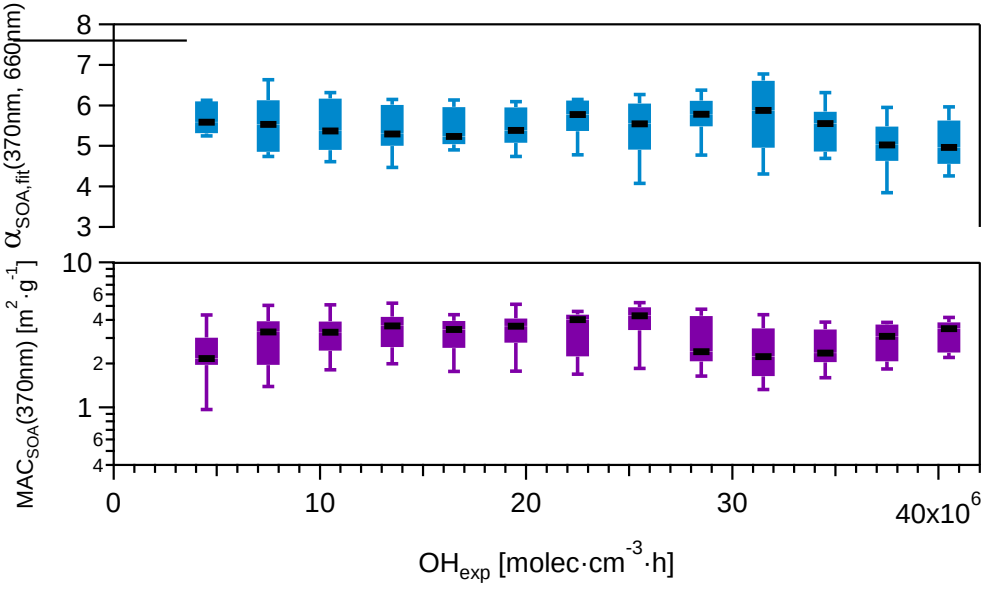

Figure 5: MAC_{SOA}(370nm) and $\alpha_{SOA,fit}$(370nm, 660nm) calculated from several smog chamber experiments plotted as a function of OH exposure. MAC_{SOA}(370nm) was obtained using Equation 19. $\alpha_{SOA,fit}$(370nm, 660nm) was obtained from fitting the MAC_{SOA} values in the range 370-660 nm for the different experiments against the wavelength. $\alpha_{SOA,fit}$(370nm, 660nm) is the slope of the linear fit applied after log transforming the data. $MAC_{SOA}(\lambda)$ for higher wavelengths are shown in figure S10.

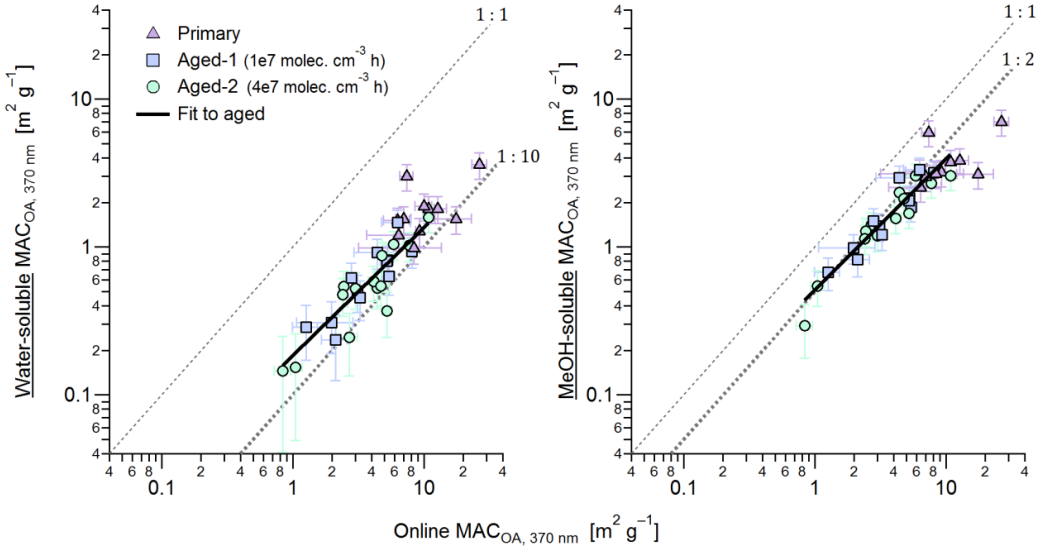

Figure 6: Comparison of the MAC_{OA}(370nm) of aged aerosols determined from online and offline measurements of absorption. The offline filter extraction method directly quantified properties of total OA (ordinate), while the average of MAC_{SOA} and MAC_{POA} from the online measurements weighted with respective mass concentrations is shown on the abscissa. (A) offline measurements of water-soluble OA, (B) methanol-soluble OA.

Atmos. Chem. Phys. Discuss., https://doi.org/10.5194/acp-2018-159
Manuscript under review for journal Atmos. Chem. Phys.
Discussion started: 13 April 2018

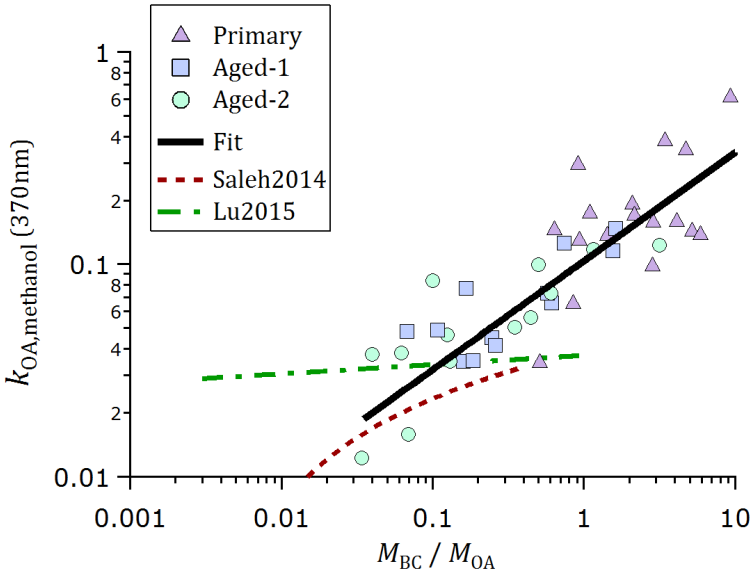

811

812 **Figure 7: Imaginary part of the OA refractive index at 370 nm, obtained from offline UV/vis spectroscopy of methanol**
813 **OA extracts, plotted as a function of f_{OA}. The ordinary least-squares fit is $\log(k_{OA,370}) = \log(M_{BC}/M_{OA})(0.51 \pm 0.07) + (-0.98 \pm 0.05)$.**

814

815

816

817

818

Atmos. Chem. Phys. Discuss., https://doi.org/10.5194/acp-2018-159
Manuscript under review for journal Atmos. Chem. Phys.
Discussion started: 13 April 2018

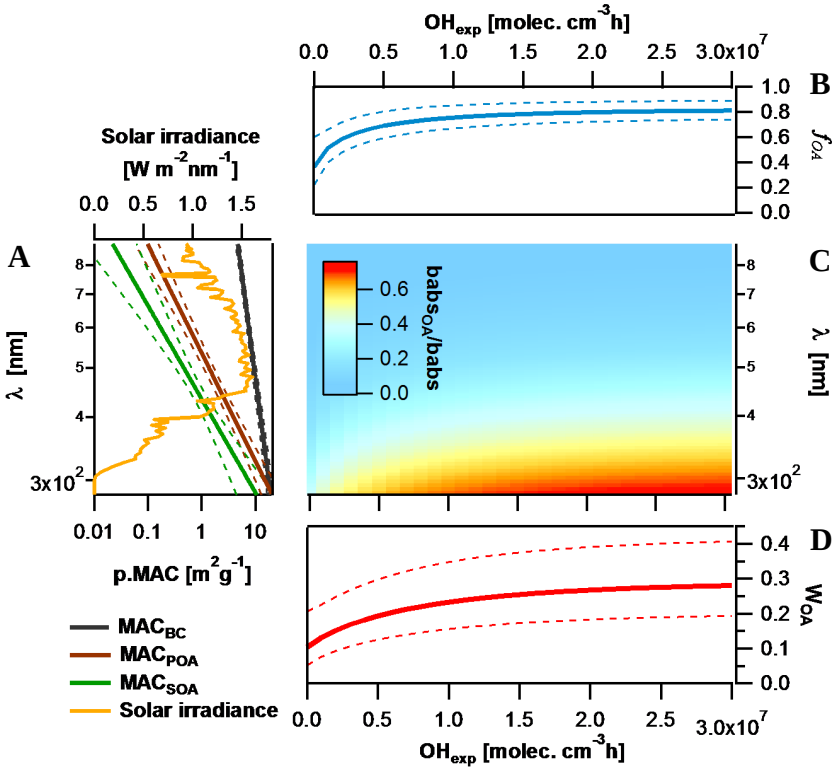

Figure 8: Impact of BrC absorption on total primary and secondary wood-burning-aerosol absorption. (A) MACs of different particle components (BC, POA and SOA) along with their corresponding standard deviations plotted as a function of wavelength based on smog chamber data and compared to the solar irradiance spectrum. (B) Species average relative abundance in the smog chamber (f_{OA}) plotted as a function of the OH exposure. (C) Image plot showing the OA absorption coefficient relative to the total aerosol absorption as a function of wavelength and OH exposure. (D) Rate of energy transfer due to BrC light absorption relative to the total carbonaceous aerosol absorption (W_{OA}) estimated as a function of aging using the solar flux, the fractions of the different components and their MACs.

Atmos. Chem. Phys. Discuss., https://doi.org/10.5194/acp-2018-159
Manuscript under review for journal Atmos. Chem. Phys.
Discussion started: 13 April 2018

Atmospheric Chemistry and Physics Discussions

837 **Table 1: Geometric mean and standard deviations of the determined MACs of BC, POA and SOA at different**
838 **wavelengths. Uncertainties were obtained from fits of Equation 13 for $MAC_{BC,}$ MAC_{POA}, while for MAC_{SOA} uncertainties**
839 **GSD values are geometric standard deviation values on the MAC_{SOA} average values from all experiments. These**
840 **uncertainties do not include uncertainties related to the determination of MAC_{BC}(880nm). By definition, BrC absorbance**
841 **at 880 nm is zero.**

	BC		POA		SOA	
λ (nm)	GM (m^2 g^{-1})	GSD	GM (m^2 g^{-1})	GSD	GM (m^2 g^{-1})	GSD
370	13.7	1.1	5.5	1.21	2.2	1.39
470	10.5	1.06	1.9	1.45	0.72	1.61
520	9	1.04	1.1	1.49	0.34	1.75
590	7.6	1.03	0.67	1.42	0.2	1.97
660	6.5	1.01	0.37	1.41	0.09	2.42
880	4.6	0.7	0*		0*	

842 *By definition

843